THERMAL AGEING OF MINERAL AND PROTEINACEOUS FOULING LAYERS DURING THE GROWTH PHASE

***L. Schnöing[1], W. Augustin[1] and S. Scholl[1]**
[1] Technische Universität Braunschweig, Institute for Chemical and Thermal Process Engineering,
Langer Kamp 7, 38106 Braunschweig, Germany
E-mail: l.schnoeing@tu-braunschweig.de

ABSTRACT

When fouling occurs in heat exchangers the characterisation and interpretation of thermal effects can be complicated due to ageing phenomena within the deposited fouling layer. Depending on the prevailing process temperatures between the liquid bulk and heat-transferring surfaces, a large thermal conductivity distribution exists according to the position of the layer within the deposit. During the growth phase fouling layer formation and ageing interact with each other. To get a deeper understanding of these occurrences, deposition and ageing should always be considered in combination.

This paper discusses an experimental method to determine temperature-dependent ageing, expressed by a change in thermal conductivity with time and along the cross section of the fouling layer. Therefore an experimental set up including a newly developed flow channel and an experimental implementation of an ageing model is presented. In first experiments proteineaceous and mineral fouling layers of whey protein concentrate (WPC) and simulated milk ultra filtrate (SMUF) were generated for different durations and thus different thicknesses. It can be shown that thermal conductivity near the heat transfering surface increases rapidly compared to the thermal conductivity of an entire fouling layer. These findings can be related to the temperature within the sublayers.

INTRODUCTION

Fouling and Ageing

The unwanted formation of deposits on heat-transferring surfaces, the so-called fouling, is a significant problem in terms of process engineering and economics in almost all areas of the process industry [1]. The negative effects of fouling include higher investments due to oversizing of apparatus, increased energy costs, reduced product quality, frequent maintenance because of cleaning, accelerated corrosion or safety aspects [2, 3]. The resulting costs are estimated at 0.25 - 0.3 % of the respective gross domestic product (GDP), which results in costs of several billion Euro/a each in the industrialised countries [3, 4]. Therefore, there is a great interest in deepening the understanding of the fouling mechanisms.

According to Epstein (1983), the various fouling mechanisms can be related to individual steps of the fouling process in a matrix: initiation, transport, deposition, removal and ageing [5]. Based on this, Ishiyama et al. (2009) conducted a survey on research priorities and needs. It was evident that corrosion and ageing require the most considerable research [6].

Ageing of deposits is relevant for various reasons. It influences the heat transfer as well as the ability to clean fouling layers due to changes in its structure or even compound. If the material adheres to the surface, the wall temperature leads to several changes [7]. It can cause changes in the chemical or morphological structure, e.g. through dehydration or polymerisation [8]. These transformations are particularly influenced by temperature in two aspects. On the one hand, the temperature within the deposit determines the properties such as structure and strength [9]. On the other hand, an increased surface temperature at the deposit-fluid-interface causes further layer growth, which in turn leads to a change of the temperature inside the deposit. Additionally the ageing of deposit is influenced if there is a constriction of the free flow cross-section during the layer growth phase and thus an increase in wall shear stress. A description or even modelling of the heat transfer is difficult in these cases, so that the different effects have to be considered carefully.

Studies of ageing phenomena

There have been several studies on the effects of ageing phenomena on heat transfer during crude oil fouling. Nelson (1934) and Atkins (1962) described temperature-dependent structural changes [10, 11] that can be attributed to changes in reaction kinetics [12]. However, the authors did not consider the temperature gradient across the fouling layer. This is inducted in the two-layer ageing model [11] and the distributed model [13]. Both models describe the thermal effect by the variable temperature-dependent thermal conductivity during crude oil fouling, which is determined by the local

ISBN: 978-0-9984188-1-0; Published online www.heatexchanger-fouling.com

temperature within the layer. The *two-layer ageing model* assumes two layers (e.g. coke and gel in crude oil fouling) of different material properties, whose boundary interface is shifted by a temperature-dependent phase change [11]. In comparison, the *distributed ageing model* assumes that the properties of individual sublayers change at different rates [6].

$$\lambda_{f,i}^{t} = \lambda_{f,i}^{\infty} + \left(\lambda_{f,i}^{o} - \lambda_{f,i}^{\infty}\right) \cdot y_i^t \qquad (1)$$

$$\frac{dy_i^t}{dt} = -k_i^t \cdot y_i^t \qquad (2)$$

In this model it is assumed that the changing thermal conductivity λ_f of each fouling sublayer i at time t can be described with a youth variable y_i^t in the range of $0 \leq y_i^t \leq 1$. The rate constant k_i^t should follow an Arrhenius approach. The reaction order of the phase change is deciding for the applicability of the ageing models for describing the deposit situation [14].

Nevertheless, these models have not yet been compared with experimental data or transferred to other foulants such as proteins or minerals.

MATERIAL AND METHODS

Flow channel test rig

There is a need of a tailored test rig to analyse the ageing behaviour of various fouling layers in different fouling phases. The below flow channel allows to identify certain fouling and ageing phenomena as mentioned before. The flow diagram in Fig. 1 shows the components of the experimental set-up.

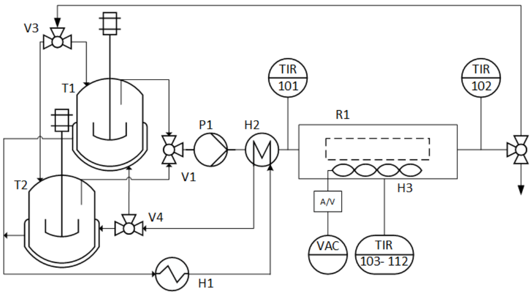

Fig. 1. Experimental set-up to generate fouling layers.

The test solution is filled in vessel T1. At the start the second vessel T2 is used for the thermal preconditioning of the test rig by filling it with deionized water. Starting from vessel T1 or T2 (controlled via V1), the solutions are fed through the electrically heated flow channel R1 by an eccentric screw pump P1 and can either flow back into the reservoir via valve V2 or be discarded (closed loop vs. open loop). The inlet temperature to the channel R1 is controlled by the thermocouple TIR101 and a preheater H2. The heat required for this is supplied by a thermostat H1. This allows precise adjustment and a short response time for temperature control and compensation of the temperature losses in the feed line. The heating circuit is then divided (with valve V4) to the two double-walled vessels to keep the bulk temperature at a constant level. The flow channel was designed for a laminar flow to investigate fouling and ageing phenomena and mechanisms precisely. It is illustrated in Fig. 2.

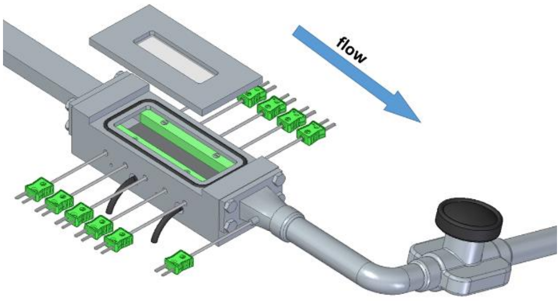

Fig. 2: Newly developed laminar operating flow channel.

The flow channel is made of stainless steel to be resistant to common cleaning solutions like sodium hydroxide or citric acid. Sample plates with dimensions of 80 mm x 20 mm x 2 mm can be inserted into the bottom of the flow channel chamber. The dimensions of the channel are 17 mm width and 7 mm height when the lid is closed. The sample plates are fixed by lateral heat-insulating clamping bars made of NECURON®. These shall mainly ensure that the fouling-inducing heat flow only comes from below the sample plates. The heat is induced by four small heating bars which are arranged crosswise to the flow. They are 8 mm in diameter and are placed 10 mm below the heat transferring surface. The flow channel can be operated up to a Reynolds number of $Re \approx 775$. Therefore an inlet length of 0.36 m was realised, required for a fully developed flow pattern.

Basically, the channel can be operated in two modes. i) in open mode the lid is removed. Therefore the outlet of the channel has a 2 mm larger diameter to ensure an undisturbed outlet flow. As a result, the liquid level can be kept relatively constant. Due to the length of the flow path (inlet and channel) the change of the liquid level in the heating zone is less than 3 % and can be neglected. In combination with an open mode, the fouling layer formed does not experience any increase in shear force due to a decrease in cross-section. ii) in closed mode, the lid of the channel is installed. Here, clamp closures with a contact pressure of 50 N ensure a quick and easy opening and closing. In the closed mode, the influence of increased shear forces on fouling and ageing phenomena can be investigated by increasing the flow velocity (caused by local fouling or set by the pump). The needle valve in the outlet serves to regulate the liquid level to fill the entire channel cross section in case of lower flow velocities. In addition to the fluid dynamic characterisation, the flow channel is equipped with one thermocouple each for the inlet and outlet and ten local thermocouples below the heat transferring surface (see Fig. 3) for the thermal characterisation.

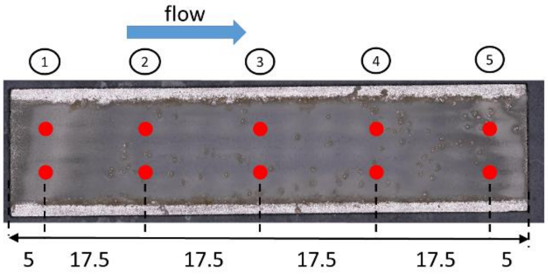

Fig. 3. Order of the ten local thermocouples 2.5 mm below the heat transferring surface. They are arranged 10 mm next to each other lateral to the flow direction and 17.5 mm in flow direction.

The flow channel uses an electric heater to allow an accurate measurement for surface temperature at the interface to the liquid flow during the deposition of foulants. Due to the constant heat flux the surface temperature of the foulant adjacent to the bulk fluid remains constant over the test run which guarantees the same conditions to the top layer relevant for the deposition. With this the temperature gradient within the layer which causes the ageing effect can be adequately determined via the wall thermocouples and attributed to the properties of the fouling layer without making any approximations about the bulk temperature.

In addition, the fouling layer is only exposed to a temperature profile in the bulk phase over the length of the sample plate (corresponds to the top layer). The conditions of the bottom layer, on the other hand, can be regarded as constant, which is a big advantage compared to fluidic heating.

Experimental implementation of ageing models

To determine the properties according to the heat transfer through fouling layers and to apply the mentioned ageing models a tailored experimental procedure is required. In the following a new experimental approach to validate ageing models is presented (see Fig. 4).

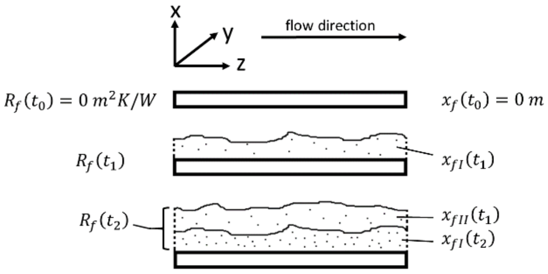

Fig. 4. Principle for the experimental procedure to investigate ageing.

The entire aged fouling layer is regarded as being composed of discrete sublayers with a certain layer thickness $x_{fI,II,...}(t_{0...i})$, changing in their properties. Three assumptions are made: i) the layer thicknesses of the sublayers do not change due to ageing (eq. 3); ii) the properties (in particular the thermal conductivity $\lambda_{fI}(t_i)$) of the first deposited layer, which is defined as the bottom layer $x_{fI}(t_{0...i})$ is not constant (due to the increasing temperature at the heat transferring surface); iii) the top layer $x_{fI,II...}(t_1)$ has the properties equal to the start (eq. 3), since the conditions of the bulk phase do not change.

$$x_{fI}(t_1) = x_{fI}(t_2) \text{ und } \lambda_{fI}(t_1) = \lambda_{fII}(t_1) \quad (3)$$

Based on these assumptions there are several sublayers between the top and the bottom layer which are defined as intermediate layer. Consequently, the individual sublayers are experimentally accessible by carrying out fouling experiments of different times and thus layer thicknesses.

Fouling experiments

Fouling experiments using whey protein concentrate with and without simulated milk ultra-filtrate (WPC plus SMUF and WPC) were carried out. For the WPC experiments 121 g of WPC were stirred into 2.2 L deionized (DI) water at max. 60°C on a heating plate until the proteins were completely dissolved. Then the solution is filled into the vessel T1. For the WPC plus SMUF solution the WPC is first dissolved in 1.6 L DI water and is filled into T1. According to Boxler (2014), three SMUF stock solutions are prepared and stored for at least 24 h at 5°C [15]. 200 mL of each stock solution are mixed so that the 600 mL solutions can be filled into T1. T2 is filled with about 1.5 L of deionized water and is used for thermal preconditioning of the test rig. The DI water is degassed for at least 15 minutes in an ultrasonic bath before the start of the experiment to avoid gas bubbles on the heat transfer surface.

Before the actual fouling experiments starts, the test rig is operated with the DI water from vessel T2 until the desired thermal process conditions (inlet temperature and wall temperatures) are reached. Thus a correct overall heat transfer coefficient of the clean surface can be calculated (see figure 6). The flow is kept constant at 63.4 mL/min. This is accompanied by a constant liquid level of 3 mm over the test plates leading to a laminar flow regime with Re ≈ 250.

When the desired temperature has reached its steady state, the feed was changed via valve V1. After switching to the test solution, it reaches the flow channel and thus the heated zone after about 106 seconds. The residence time of foulants in the chamber is 3.9 s. The fluid is fed back into the vessel via the valves V2 and V3. Over a longer time the WPC solution is accumulated in the vessel T2 during the experiments. Therefore T2 could also be used to generate fouling layer. As a result many fouling layers were produced within a short time. Following this, the unknown protein concentration in the bulk phase was not considered in this work.

However, the test plates together with the fouling layers can be removed and replaced from the flow channel at any time for *ex situ* examination. The same applies to the placement of new clean surfaces. During this handling the pump did not have to be switched off due to the slow flow rate of the test solutions. The process condition and the number of fouling layers generated at a power input of 140 W are listed in Table 1.

Table. 1. Process condition and the number of fouling layers (NoFL) generated and used to investigate the thermal conductivity (see figure7 and 8).

Foulant	NoFL	T_{in} / °C	q / kW/m^2
WPC	8	62.2 (±0.6)	45.8 (±0.8)
	5	67.0 (±0.1)	44.2 (±3.3)
WPC plus SMUF	9	62.8 (±0.1)	46.1 (±0.3)

The power input into the fluid relevant for fouling (respectively the effective heat flux q) was calculated using the following equation.

$$q = \dot{m} \cdot c_p \cdot \left(T_{b,out} - T_{b,in}\right) \cdot A^{-1} \qquad (4)$$

In this equation $\dot{m}$ is the mass flow through the flow channel with its corresponding heat capacity c_p. $T_{b,out}$ is the measured temperature in the bulk outlet while $T_{b,in}$ is the inlet temperature. A represents the heat transferring surface area. Thus the average efficiency of the flow channel is about 31.1 % for the experiments carried out. The thermal fouling resistance can be calculated by the temperature of the ten local thermocouples as follows:

$$R_{f,th} = \frac{1}{U_f} - \frac{1}{U_0} = \frac{T_{w,t} - T_{w,0}}{q} \qquad (5)$$

Characterisation of fouling layer

Fouling layer thickness

The aim of this work is to link the measured thermal fouling resistance via thermocouples to the corresponding fouling layer thickness. Therefore it is important to measure both values at the same location. The fouling layer thickness is measured at a precise location by using a digital microscope.

The sample plate is placed below the digital microscope and a fixed point (upper corner) is defined as zero. Starting from this position, the location of the temperature measuring positions can be approached precisely. As mentioned before, the temperatures are measured at ten positions, which together represent five locations in the direction of flow each with two measuring positions. In order to obtain a representative layer thickness for a certain area, five areas $A_{f,i}$ are defined for which mean layer height is then determined. This is illustrated in Fig. 5 for the 4th location in the direction of flow; all 5 locations provides similar visual observation and only the 4th location is presented here.

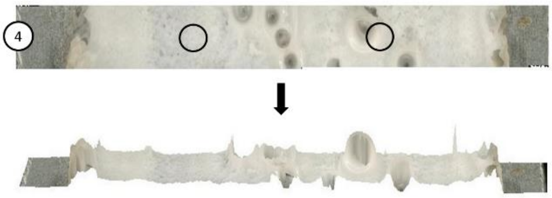

Fig. 5. Area over the sample plate of the fouling layer at the 4th location in the direction of flow. Over this area a 3D image is taken from which the volume is determined to calculate the representative fouling layer thickness. The black circles represent the positions of the thermocouples underneath the plate.

To capture the area of interest the analysis is performed by taking a series of 3D images which are composed to a 1 mm x 20 mm image. In this area, the entire surface may not be covered completely or an uneven surface topography prevails, therefore the mean layer thickness is calculated by determining the fouling volume $V_{f,i}$. Divided by the area $A_{f,i}$ this gives the average layer thickness $\overline{x_{f,\imath}}$. After taking the 3D images the fouling layer were discarded.

$$\frac{V_{f,i}}{A_{f,i}} = \overline{x_{f,\imath}} \qquad (6)$$

Thermal conductivity

The measured thermal fouling resistance compared to the corresponding fouling layer thickness allows the calculation of the apparent total thermal conductivity of the fouling layer, which should be as near as possible to the effective thermal conductivity due to the laminar flow. Therefore the mean fouling resistances $\overline{R_{f,th,\imath}}$ of two thermocouples at location $i = 1 \ldots 5$ were divided by the fouling layer thickness $\overline{x_{f,\imath}}$.

$$\lambda_{f,i} = \frac{\overline{x_{f,\imath}}}{\overline{R_{f,th,\imath}}} \qquad (7)$$

The mean fouling resistance $\overline{R_{f,th,\imath}}$ has to be regarded to the two related thermocouples. So the temperature $T_{w,t}$ for the calculation of the thermal fouling resistance (eq. 5) is based on the following eq. 8. It is determined over a period of 10 seconds at the end of each fouling cycle (see Fig. 6).

$$T_{w,t} = \frac{T_{w,t,i,right} + T_{w,t,i,left}}{2} \qquad (8)$$

RESULTS AND DISCUSSION

Thermal characterisation

In this chapter the thermal characterisation of the flow channel and the determination of the relevant fouling resistances are discussed. Fig. 6 shows the typical courses of the five thermal fouling resistances over time. A cycle of one fouling layer production is shown. This fouling layer was formed at an inlet temperature of 62.2 °C and a heating power of 140 W corresponding to an area-averaged heat flux of 45.8 (±0.8) / kW/m^2 (see Table 1).

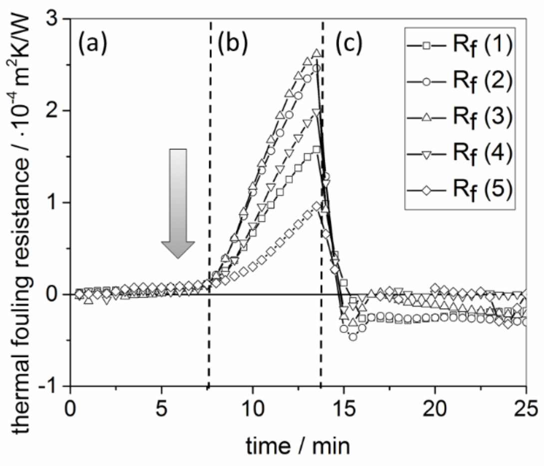

Fig. 6. Course of the thermal fouling resistance at the five locations in the direction of flow over time during the generation of one WPC fouling layer. a) shows the stationary phase, b) the fouling growth phase and c) the phase of sample removal. The arrow at 6.7 min marks the change from water to the WPC solution (by valve V1).

The typical course of the fouling resistances can be separated into three phases. The first phase (a) is the stationary phase in which the test rig is operated with DI water. In this phase the heat transfer coefficient of the clean surface is determined. This phase is followed by the growth phase (b), in which the high WPC concentration results in a very rapid and sharp increase in the fouling layer thickness respectively of the thermal fouling resistance. The aim of this work is to identify ageing by means of monitoring a change in thermal conductivity during the growth phase. Therefore this phase is defined as a fouling layer growth with no increasing removal due to a further enhanced fluid shear stress. This is given when the channel is operated without a lid that restricts or limits the flow cross section. At the end of the growth phase the highest thermal fouling resistance is obtained. The transition to the final phase (c) is clearly visible by a sudden drop in the fouling resistance. At this point the sample plate including the fouling layer has been removed. During this phase (c) the flow medium was also changed from WPC solution to water. A comparison between the fouling resistances of phases (a) and (c) shows a slight difference due to the fact that no sample plate was inserted in the last phase.

Thermal conductivity of fouling layer

In the following, the results of the overall thermal conductivity of the entire fouling layer of WPC (Fig. 7) and WPC plus SMUF (Fig. 8) are presented and discussed. Based on the measured fouling resistances and the layer thicknesses, the thermal conductivity is calculated according to eq. 7 and is shown in dependency of the layer thickness. For WPC, 65 individual data points are shown in Fig. 7 with three outliers not included. Fig. 8 presents 45 data points for the WPC plus SMUF with two outliers not included.

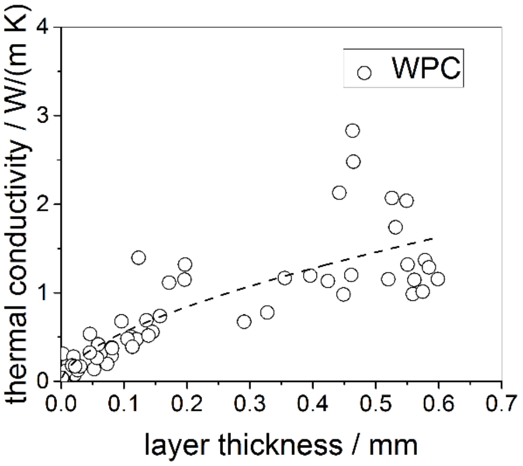

Fig. 7. Total thermal conductivity of WPC deposits at different fouling layer thicknesses.

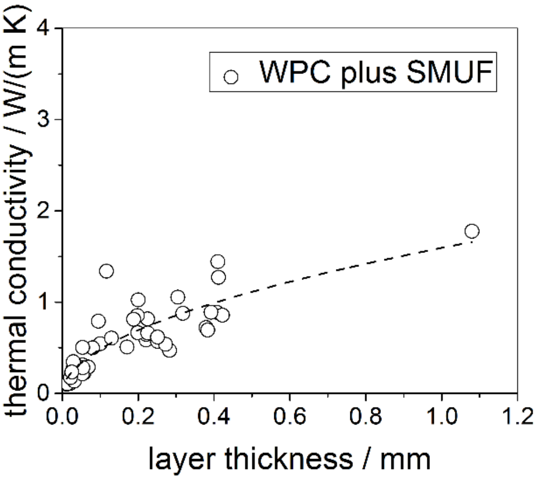

Fig. 8. Total thermal conductivity of WPC plus SMUF deposits at different fouling layer thicknesses.

Obviously the thermal conductivity λ_f of the entire fouling layer increases with the thickness x_f for both systems. Based on this, the values can be approximated using a power law approach (see Table 2) with a regression value greater than 0.8. These uncertainties are not only due to measurement and instrument inaccuracies but also to different bulk temperatures in the direction of flow. Generally this could be calculated, however, further experiments are needed for more extensive data.

Table. 2: Equation and R values for total thermal conductivity of WPC and WPC plus SMUF fouling layer depending on their thickness; λ_f in W/(mK), x_f in mm.

Foulant	Equation	R value
WPC	$\lambda_f = 2.21 \cdot x_f{}^{0.60}$	0.81
WPC plus SMUF	$\lambda_f = 1.59 \cdot x_f{}^{0.52}$	0.83

Notwithstanding the addition of SMUF the graphs show a steep increase of λ_f for x_f < 0.1 mm. Thereafter the increase flattened.

The thermal conductivity values for deposits thinner than 0.4 mm are typically below 1 W/(m K). Compared to the literature these findings are in good agreement with other authors within this range of thickness. Tuladhar et al. (2000) determined the thermal conductivity during swelling experiments of WPC deposits to ca. 0.26 W/(m K) [16]. Davies et al. (1997) obtained an effective value of 0.47 W/(m K) [17].

It is expected that the thermal conductivity lies in between those of water (0.68 W/(m K) at 90°C) and proteins (0.26 W/(m K) at 90°C) [18]. But Delaplace and Leuliet (1995) already examined that the thermal conductivity of whey protein in a plate heat exchanger could be higher as seen in this work. The authors reported an apparent thermal conductivity between 0.27 W/(m K) and 3 W/(m K), which were based on model calculations and mentioned that their fouling layers had a brown colour [19]. This is an indication for cooked and even burnt proteins which may have a higher thermal conductivity. But here further investigations are necessary. As a general trend it could be assumed that the thermal conductivity increases due to higher deposit temperatures [20]. In addition, it is also striking that the absolute thermal conductivity of WPC plus SMUF generally appears to be smaller than those of pure WPC even though the thermal conductivity of calcium phosphate, which is the main component in SMUF deposits, is about 1.039 W/(m K) [21]. It is possible that the increased content of Ca ions in the fouling layer binds more water [22], so that λ_f assumes lower values.

Due to the small sample size and the deviations of fitting, further investigations have to follow. Apart from this, these results can be used for the verification of ageing models.

Thermal conductivity along the cross secction

The ageing of deposits is accompanied by a change in thermal conductivity, especially within the fouling layer. Due to the increase in temperature from the bulk phase of the test solution to the heat-transferring surface, it is expected that the temperature-dependent properties of the deposits will also change in a similar manner. To investigate these phenomena, Fig. 9 shows the change in thermal conductivity of a 0.18 mm and a 0.6 mm thick fouling layer for the two component systems. The entire fouling layer is assumed to consist of 3 and 10 sublayers (I … III; I … X) with a thickness of 0.06 mm each. According to Table 2, these calculations are based on a thermal conductivity of 0.8 W/(m K) and 1.6 W/(m K) (WPC) as well as 0.7 W/(m K) and 1.2 W/(m K) (WPC plus SMUF) for an entire fouling layer of 0.6 mm and 1.8 mm respectively.

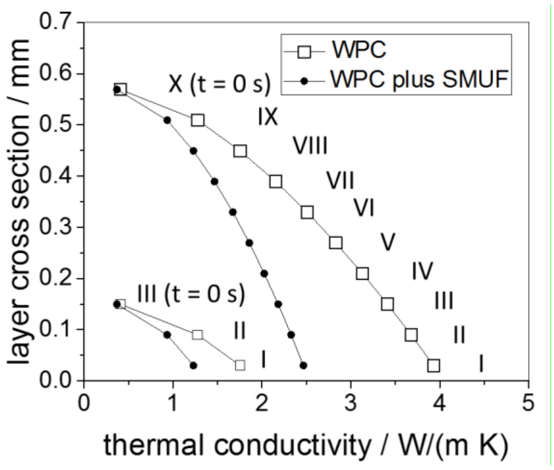

Fig. 9. Local thermal conductivity within fouling layers of 0.18 mm and 0.6 mm thickness of WPC and WPC plus SMUF. III (t = 0 s) and X (t = 0 s) represent the top layer, I always the bottom layer.

It is noticeable that the values for λ_i increase significantly towards the heat transferring surface (III→I; X→I), independent of foulant or time. When the fouling layer increases from 0.18 mm to 0.6 mm, then ageing also occurs, which can be described by the following three characteristics.

- The thermal conductivity of the uppermost fresh layers (t = 0s) remains unchanged at 0.4W/(m K) (for WPC and WPC plus SMUF);
- The thermal conductivity of the bottom layer close to the heat transferring surface increases by a factor of 2 approximately compared to λ_f;
- The upper two sublayers (X and IX) are characterised by a more significant change in thermal conductivity than the other sublayers closer to the heat transferring surface.

The assumption that the course of the thermal conductivity can be divided into two sections possibly indicates a front in which the water content is increased. Since the upper layers represents the interface to the liquid phase, it is to be expected that the water content in this part of the deposits is higher. With an obtained thermal conductivity in the top layer III (t = 0 s) (for layer of 0.18 mm) and X (t = 0 s) (for layer of 0.6 mm) the water content ε of

35 % (WPC) and 26 % (WPC plus SMUF) respectively can be assumed according to eq. 9. The data for λ_{solid} correspond to proteins and were taken from [18]. Therefore it was assumed that the thermal conductivity of the solid do not differ from WPC to WPC plus SMUF.

$$\lambda_{eff} = \lambda_{water} \cdot \varepsilon + \lambda_{solid} \cdot (1 - \varepsilon) \qquad (9)$$

From the third sublayer (VIII) onwards (for layer of 0.6 mm), there seems to be an approximately linear increase in thermal conductivity towards the heat transferring surface. Within this range, the thermal conductivity values are significantly higher than those of solid proteins or water. This phenomenon probably indicates structural changes of the deposit and should have a significant influence on the thermal properties of such fouling layers.

Temperature dependency

The change of fouling layer properties with temperature may be a strong indicator for ageing properties. Figure 10 shows an example of the calculated thermal conductivity in the bottom layer for WPC with an inlet temperature of 62.17 °C (see Table 1) as a function of the mean temperature in the bottom layer. This was determined using $T_{w,0}$ and $T_{w,t}$.

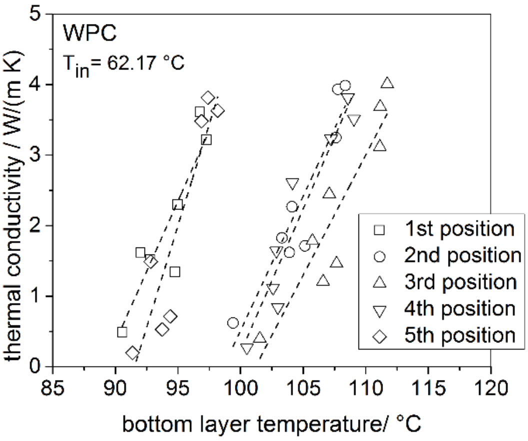

Fig. 10. Local thermal conductivity of WPC deposits in the bottom layer over mean temperature in the sublayer.

There seems to be a direct dependence between the thermal conductivity and the internal deposit temperature. This statement is supported by R-values of over 0.9 (for WPC plus SMUF R > 0.92) by linear fitting. As a result, the thermal conductivity increases linearly with increasing temperature in the investigated range. It is noticeable that no approximation of the values is possible independent of the position of the temperature measuring positions. This possibly indicates an influence of the bulk temperature. Belmar-Beiny et al. (1993) mentioned that deposition can undergo a change from surface reaction control to bulk reaction control when the protein is exposed to different temperatures [23]. However, it is also possible that exceeding a critical temperature of 100 °C is decisive for the observed dependencies. This has to be investigated in future experiments.

CONCLUSION

An experimental approach is presented to analyse ageing phenomena of food-based whey protein deposits. For this purpose a new laminar flow channel was developed (*Re* ≤ 775) and allows a precise thermal analysis of the deposition and ageing process. The determined thermal fouling resistance could successfully be linked to the layer thickness determined by a digital microscope. As a result the thermal conductivities of whey protein deposits were calculated with absolute values matching closely with literature.

Assuming that a fouling layer consists of different sublayers, it could be shown that the ageing process is characterised by increased thermal conductivity (up to a factor of 2) close to the heat transferring surface compared to the rest of the deposit. The thermal conductivity in the layer near the interface to the fluid flow (top layer) remains constant at about 0.4 W/(m K) while the layer near the heat transfer surface (bottom layer) changes by a factor of up to 9 (WPC) and 6.5 (WPC plus SMUF). This change within the deposit can be linked to the temperature prevailing at this location. However, further experiments are necessary to achieve a more precise correlation between the local thermal conductivity and the layer thickness, furthermore under increased shear forces. The water content in the deposit should be determined as well. In addition, a detailed relationship to temperature over a larger temperature range and the influence of bulk temperature has to be investigated.

ACKOWLEDGEMENT

Special thanks go to the student assistant Justus Caspar for the design drawing of the flow channel. Furthermore the ICTV mechanical workshop around the team of Karl Karrenführer and our electrician Jörg Leppelt greatly supported this work by building the flow channel and configuring the experimental setup as well as the electrical installation.

NOMENCLATURE

A	area of fouling layer, m^2
c_p	heat capacity, J/ (kg K)
k	rate constant, s^{-1}
$\dot{m}$	mass flow, kg/s
NOFL	number of fouling layer
q	heat flux, W/m^2
R_f	thermal fouling resistance, m^2 K/W
SMUF	Simulated Milk Ultra Filtrate
t	time, min
T	temperature, °C

U	overall heat transfer coefficient, W/(m^2 K)
V	volume of fouling layer, m^3
WPC	Whey Protein Concentrate
x	thickness, m
y	youth variable
ε	water content
λ	thermal conductivity, W/(m K)

Subscript

b	bulk
channel	flow channel
f	fouling
fluid	fluid
growth	growth phase
i	discrete values, stepwise parameter
in	inlet flow
I,II,...	Number of sublayer; starting from the wall
out	outlet flow
th	thermal
w	wall
0	clean surface

REFERENCES

[1] Taborek J., Knudsen J. G., Aoki T., Ritter R. B., Palen J. W., Fouling - The Major Unresolved Problem in Heat Transfer, *Heat Transf. Res. Inc.*, 1972.

[2] Bohnet M., Fouling an Wärmeübertragungsflächen, *Chem. Ing. Tech.* (57 (1)), 24 – 36., 1985.

[3] Steinhagen R., Müller-Steinhagen H., Maani K., Problems and Costs due to Heat Exchanger Fouling in New Zealand Industries, *Heat Transfer Eng.*, 14 (1), 19 – 30., 1993.

[4] Garrett-Price B. A., Fouling of heat exchangers: Characteristics, costs, prevention, control, and removal, *Noyes Publ, Park Ridge*, NJ; 1985.

[5] Epstein N., Thinking about Heat Transfer Fouling: A 5 × 5 Matrix, *Heat Transfer Eng.*, 4 (1), 43 – 56., 1983.

[6] Ishiyama E. M., Coletti F., Macchietto S., Paterson W. R., Wilson D. I., Impact of deposit ageing on thermal fouling: Lumped parameter model, *AIChE J*, 68., 2009.

[7] Coletti F., Ishiyama E. M., Paterson W. R., Wilson D. I., Macchietto S., Impact of deposit aging and surface roughness on thermal fouling: Distributed model, *AIChE J.*, 56 (12), 3257 – 3273., 2010.

[8] Watkinson A. P., Wilson D. I., Chemical reaction fouling: A review, *Exp. Therm. Fluid Sci.*, 14 (4), 361 – 374., 1997.

[9] Fickak A.; Hatfield E.; Chen X., Influence of Run Time and Aging on Fouling and Cleaning of Whey Protein Deposits on Heat Exchanger Surface, J. Food Res., 1 (1), 2012

[10] Nelson W. L., Fouling of heat exchangers, *Refiner & Natural Gasoline Manufacturer*, 13(7), 271-276; 13(8) 292-298, 1934.

[11] Atkins G. T., What to do about high coking rates, *Petro/Chem Engineer* (34(4)), 20 – 25, 1962.

[12] Jones E. G., Balster W. J., Surface Fouling in Aviation Fuel: Short- vs Long-Term Isothermal Tests, *Energy .Fuels*, 9 (4), 610 – 615, 1995.

[13] Crittenden B. D., Kolaczkowski S. T., O'Callaghan P. W., Energy savings through the accurate prediction of heat transfer fouling resistances, Energy for Industry. London: *Pergamon Press*, 257 – 266, 1979.

[14] Ishiyama E. M., Paterson W. R., Wilson D. Ian, Exploration of alternative models for the aging of fouling deposits, *AIChE J.*, 57 (11), 3199 – 3209, 2011.

[15] Boxler C., Augustin W., Scholl S., Composition of milk fouling deposits in a plate heat exchanger under pulsed flow conditions, *J. Food Eng.*, 121, 1 – 8, 2014.

[16] Tuladhar T. R., Paterson W. R., Wilson D. I., Thermal Conductivity of Whey Protein Films Undergoing Swelling, *Food and Bioprod. Process.*, 80 (4), 332 – 339, 2002.

[17] Davies T. J., Henstridge S. C., Gillham C. R., Wilson D. I., Investigation of Whey Protein Deposit Properties Using Heat Flux Sensors, *Food and Bioprod. Process.*, 75 (2), 106 – 110, 1997.

[18] Delplace F., Leuliet J. C., Modelling fouling of a plate heat exchanger with different flow arrangements by whey protein solutions, *Food Bioprod. Brocess. Trans. Inst. Chem. Eng., Part C*, 1995.

[19] Fricke B., Becker B., Evaluation of Thermophysical Property Models for Foods, *HVAC&R Res.*, 7 (4), 311 – 330., 2001.

[20] Chen J., Temperature-Dependent Dielectric and Thermal Properties of Whey Protein Gel and Mashed Potato, *Trans. ASABE*, 1457 – 1467, 2013.

[21] Singh A., Heat exchanger fouling by precipitation of calcium phosphates, The University of British Columbia., 1992.

[22] Khaldi M, Blanpain-Avet P, Guerin R, Ronse G, Bouvier L, André C, Bornaz S, Croguennec T, Jeantet; R, Delaplace G., Effect of calcium content and flow regime on whey protein fouling and cleaning in a plate heat exchanger. *J. Food Eng.*, 147, 68 - 78, 2015.

[23] Belmar-Beiny M. T., Gotham S. M., Paterson W. R., Fryer P. J., Pritchard A. M., The effect of Reynolds number and fluid temperature in whey protein fouling, *J. Food Eng.*, 19 (2), 119 – 139, 1993.